Available online at www.sciencedirect.com

SciVerse ScienceDirect

Journal of the European Ceramic Society 32 (2012) 1163–1173

www.elsevier.com/locate/jeurceramsoc

Toughness measurement on ball specimens. Part I: Theoretical analysis

Stefan Strobl [a,b,*], Peter Supancic [a,b], Tanja Lube [a], Robert Danzer [a]

[a] *Institut für Struktur- und Funktionskeramik, Montanuniversitaet Leoben, Peter-Tunner-Straße 5, A-8700 Leoben, Austria*[c]
[b] *Materials Center Leoben Forschung GmbH, Roseggerstraße 12, A-8700 Leoben, Austria*[d]

Received 26 August 2011; received in revised form 23 November 2011; accepted 5 December 2011
Available online 5 January 2012

Abstract

A new toughness test for ball-shaped specimens is presented. In analogy to the "Surface Crack in Flexure"-method the fracture toughness is determined by making a semi-elliptical surface crack with a Knoop indenter into the surface of the specimen. In our case the specimen is a notched ball with an indent opposite to the notch. The recently developed "Notched Ball Test" produces a well defined and almost uniaxial stress field.

The stress intensity factor of the crack in the notched ball is determined with FE methods in a parametric study in the practical range of the notch geometries, crack shapes and other parameters. The results correlate well with established calculations based on the Newman–Raju model.

The new test is regarded as a component test for bearing balls and offers new possibilities for material selection and characterisation. An experimental evaluation on several ceramic materials will be presented in a consecutive paper.

Keywords: Fracture; Mechanical properties; Toughness and toughening; Si_3N_4; Notched Ball Test

1. Introduction

Structural ceramics, especially silicon nitride (Si_3N_4), are distinguished due to their special properties: low wear rates, high stiffness, low density, electrical insulation and high corrosion resistance. For this reason they are advantageous for highly loaded structural applications or when special properties (due to additional requirements) are needed. An important application with a rapidly growing market are hybrid bearings (ceramic rolling elements and metal races), which are used for high operation speeds (e.g. racing), current generators (e.g. in wind turbines) or in the chemical industry.[1,2] Key elements of the bearings are the ceramic rolling elements, which should have to comply with highest requirements. But relevant standards for the proper determination of the mechanical properties of roller elements are missing.

Mechanical properties of ceramics depend to a large fraction on their microstructure, which is strongly influenced by processing conditions. Therefore proper mechanical tests should be made on specimens cut out of the components, or – even better – on components themselves. The strength depends on the flaw populations occurring in the component which are – in general – different in the volume and at the surface. In roller bearing applications the highest tensile stresses occur at (and near) the surface of the rolling elements and surface flaws are of outmost significance for the strength of rolling elements. Therefore the highest loaded area in mechanical testing of bearing balls should be situated at the surface of the balls.

These conditions are fulfilled in the case of the Notched Ball Test (NBT)[3–6] for the strength measurement of balls, which has recently been developed by several of the authors. A slim notch is cut into the equatorial plane of a sphere and the testing force is applied on the poles perpendicular to the notch. In that way an almost uniaxial tensile stress field is generated in the surface near area opposite the notch, which is used for the determination of the strength of the Notched Ball (NB) specimen. Therefore the NBT is very sensitive to surface flaws and relevant for determining the strength of ceramic balls. Note that a similar test, the C-Sphere Test,[7] was proposed earlier, where the notch is not slim but wide and must have a precise shape. The quality of bearing balls is strongly related to a high toughness, which should also be measured at specimens cut out of the balls or on the balls themselves. In industry toughness measurements on

* Corresponding author at: Institut für Struktur- und Funktionskeramik, Montanuniversitaet Leoben, Peter-Tunner-Straße 5, A-8700 Leoben, Austria.
Tel.: +43 3842 402 4113; fax: +43 3842 402 4102.
E-mail address: stefan.strobl@mcl.at (S. Strobl).
[c] isfk@unileoben.ac.at, http://www.isfk.at.
[d] mclburo@mcl.at, http://www.mcl.at.

0955-2219/$ – see front matter © 2011 Elsevier Ltd. All rights reserved.
doi:10.1016/j.jeurceramsoc.2011.12.003

bearing balls are commonly made with indentation methods (i.e. "Indentation Fracture"-method[8–12] due to their ease of use. It has been recognised in the last years that the toughness values measured with indentation methods depend on the size and shape of the plastic deformation zone around the indent, which may vary from material to material. Therefore the resulting "Indentation Fracture Resistance" (IFR) is only a rough estimate of fracture toughness and has to be calibrated for each material and indentation load.

Standardised fracture toughness testing methods normally use standard beams, which contain a well defined crack and which are loaded and broken in 4-point bending. The fracture toughness K_C is determined by application of the Irwin failure criterion: $K = K_C$, where K is the stress intensity factor (SIF). Note that K and K_C mean pure Mode I configuration (i.e. crack opening). In the following the authors disclaim to use indices because the other loading Modes are not discussed. The critical stress intensity factor can be determined using the fracture load and with information on beam and crack geometry.

A prominent example is the "Single Edge V-Notched Beam" (SEVNB) method,[13] in which, a slim notch is introduced in a bending beam using a razor blade. In that way straight notches with a tip radius of at least 3 μm can be produced. For materials having a mean grain size of several micrometers or greater, this is an accurate approximation of a crack[14,15] but for fine grained materials sharper cracks would be beneficial for a precise toughness measurement.

Very sharp cracks are used in the "Surface Crack in Flexure" (SCF) method.[16,17] A Knoop hardness indent is made on the tensile loaded side of a rectangular bending bar. Thus, an almost semi-elliptical and very sharp crack is introduced in the surface. The size of the remaining Knoop crack is determined by fractographic means, which may need some fractographic experience.

In comparison the SEVNB method is easier to apply and less time consuming but the SCF-method is more appropriate for materials with a very fine grain structure.

To measure the fracture toughness of ceramic balls, bending bars can machined out of balls, if the balls have minimum diameter, say 20–25 mm, but most of the produced rolling elements are smaller. So a simple toughness test for ball shaped components is needed. In this work we will focus on an extension of the SCF method on NB specimens.

2. The SCF-method applied to notched ball specimens

2.1. The Notched Ball Test for strength measurement

Recently, the "Notched Ball Test" (NBT) was established at the Institut für Struktur- und Funktionskeramik at Montanuniversitaet Leoben to measure the strength of ceramic balls, see Fig. 1. With a commercial diamond disc, a notch is cut into the equatorial plane of the ball (depth ca. 80% of the diameter) and the load F is applied at the poles (point 3) using a conventional testing machine. Then the notch is squeezed together and high tensile stresses occur in the surface region of the ball opposite to the notch root (the maximum stress σ_{NBT} is located at position 1, furthermore called peak stress).

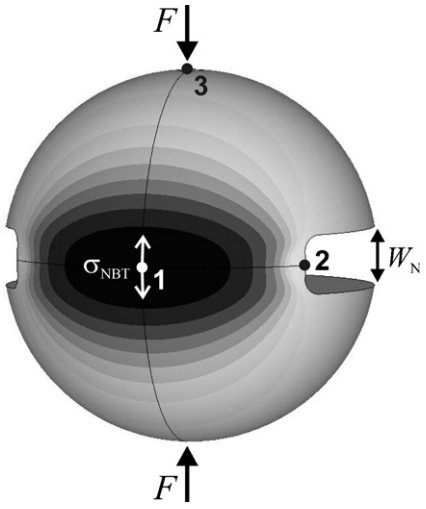

Fig. 1. Stress distribution of a notched ball (NB) specimen. The ball is loaded in compression with the force F perpendicular to the notch. This causes tensile stresses in the outer surface region of the ball opposite to the notch with a maximum stress σ_{NBT} at position 1. W_N is the notch width. Adapted from [6].

The stress field in the NB only depends on the ball diameter D (ball radius R), the notch length L_N, the notch width W_N, the fillet radius R_N of the notch at the notch base, and on the Poisson's ratio ν of the tested material. The geometric parameters are defined in Figs. 1 and 2.

To generalize the results the definition of the following dimensionless geometric parameters is convenient: the relative notch length $\lambda = L_N/D$, the relative width of the notch $\omega = W_N/D$, the relative radius of the fillet of the notch base $\rho = R_N/W_N$.

The peak stress σ_{NBT} can be calculated using Eq. (1), with h as the ligament thickness and f_N as dimensionless factor, which depends on the relative notch geometry (λ, ω, ρ) and the Poisson's ratio ν, and which, in the parameter range used for tests,

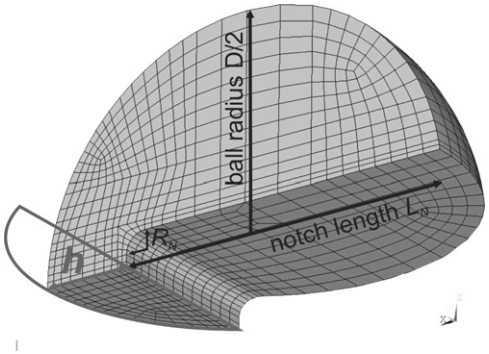

Fig. 2. The stress field in the specimen depends on the ball diameter D, the notch length L_N, the notch width W_N and the fillet radius R_N of the notch. The dimensionless geometric parameters are the relative notch length $\lambda = L_N/D$, the relative width of the notch $\omega = W_N/D$, the relative radius of the fillet of the notch base $\rho = R_N/W_N$. In the equatorial plane remains a ligament having the shape of a segment of a circle with the thickness $h = D - L_N$.

is $0.4 \leq f_N \leq 1.5$. A detailed analysis of f_N for a wide range of relative parameters can be found in.[6]

$$\sigma_{NBT} = f_N \times \frac{6F}{h^2} \quad \text{with} \quad f_N = f_N(\lambda, \omega, \rho, \nu) \tag{1}$$

The sample preparation is clearly specified and the geometry measurement of the NB specimen is precisely feasible. The simple testing setup minimizes measurement errors caused by inaccurate alignment. Because the loading point is far away from the area, where the maximum tensile stress occurs (and which is used for strength testing), the result is only very little influenced by the local contact situation (contact stresses). Furthermore friction is extremely reduced (in comparison to bending testing; here friction may have a very strong impact on stress determination) and can be neglected for data evaluation.

In summary the NBT is a very precise and simple testing method, which makes the characterisation of original ball surfaces possible. Up to now almost 1000 NB-tests on specimens having different diameters and relative notch geometries, and are made from different materials have been successfully tested in the laboratory of the authors.[3–6,18]

2.2. Basic principles and fracture toughness determination

The common approach in fracture toughness testing for ceramic materials is based on the Griffith/Irwin fracture criterion:

$$K_C \geq K = \sigma Y \sqrt{a\pi}. \tag{2}$$

K_C is the Mode I fracture toughness, K is the stress intensity factor, σ is a reference stress in the uncracked specimen (e.g. outer fibre stress for bending), a is the size of the crack and Y is a geometric factor, which is determined by the geometry of the specimen, the crack shape and the course of the stress field. For details see standard text books on fracture mechanics or on mechanical properties of ceramics.[19,20] Information on geometric factors for typical loading cases and standard specimen geometries can be found in literature.[21]

To apply this equation for fracture toughness determination, a well defined stress field, which contains a crack of well-known geometry and size, is needed. In the case of the standardized SCF-method[16,17,22,23] a surface crack is produced with a Knoop indent in a bending bar specimen. The indent causes plastic deformation around the indented zone, which also causes unknown internal stresses. They are relaxed by removing the plastic deformed material by grinding-off a thin surface layer of the specimen's surface, in which the hardness impression was made. Then the specimen is loaded in four point bending, i.e. a well defined (known) stress field is applied. The load is increased until fracture occurs.

After fracture the crack size is determined on the fracture surface by fractographic means. It has a semi-elliptic shape. For a material with the Poisson's ratio $\nu = 0.3$ Newman and Raju[24–26] have developed a parameterized and generalized solution of the geometric factor Y of a semi-elliptic crack in the stress field of a bent bar (thickness t and width $2b$). It depends on the geometry of the crack (crack width $2c$, crack depth a), the bar's cross-section

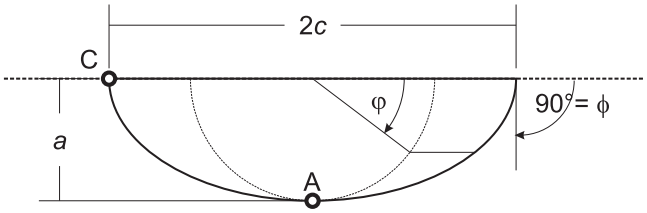

Fig. 3. Schematic of a semi elliptical crack. The crack width $2c$ at the surface and the crack depth a are indicated as well as the points A ($\varphi = 90°$) and C ($\varphi = 0°$), where the geometry factor Y can reach a maximum.

and on the position at the crack front given by the angle φ, see Fig. 3. The geometric factor $Y(a, t, b, c, \varphi)$ shows a maximum either in point A (deepest point of the crack) or in point C (crack front intersection with the specimen surface). In the following these special values of the geometric factor are called Y_A and Y_C. Tentatively $Y_A > Y_C$ for shallow cracks ($c > a$) and vice versa. Of course fracture is initiated at the position the largest stress intensity factor.

The SCF-method can be adopted for the loading situation in a NB specimen. The stress distribution in the NB specimen is well-known and similar to that in a conventional four point bending bar, i.e. almost uniaxial. The Knoop indent is introduced opposite to the notch, where the maximum stress occurs (position 1), see Fig. 4. In the following, the plastically deformed surface layer is ground off and the NB specimen is broken. For the evaluation of fracture toughness, the stress field of the NB specimen after grinding-off the plastically deformed surface layer has to be determined. Then the geometric factor of a semi-elliptical crack in that stress field has to be determined. Again the crack size and geometry will be measured by fractographic means.

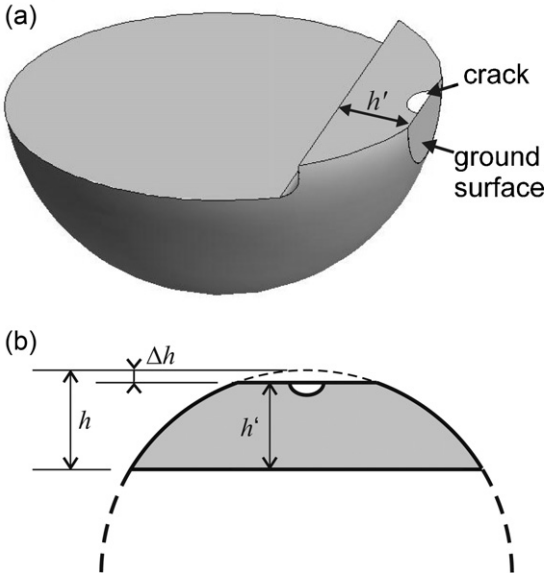

Fig. 4. Illustration of notched ball (half model) with a semi-elliptical crack (white) and ground down to remove the plastic zone around the indent. The remaining ligament thickness is ($h' = h - \Delta h$).

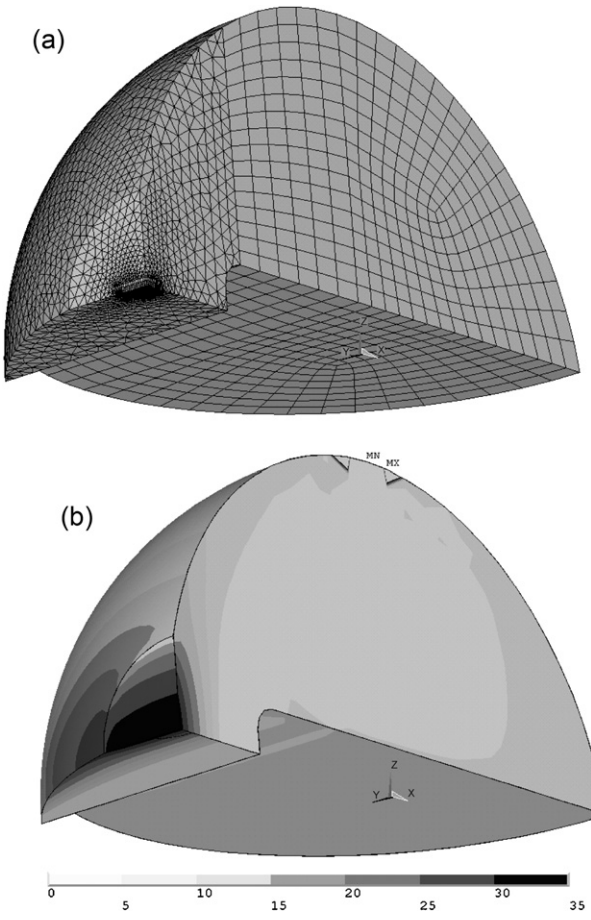

Fig. 5. Reference model of a ground-off notched ball specimen used for the parametric study: (a) mesh overview and (b) stress distribution (σ_z) without crack (compare with Fig. 1). Stress values given in MPa for an applied load of $F = 1$ N.

2.3. Stress distribution in the NB specimen due to material removal

As in the case of SCF measurements on bending bars, the plastically deformed material in the surface of the ball around the indent has to be removed. The thickness of the removed surface layer (removal depth) is called Δh, or in relative units $\alpha = \Delta h/R$, see Fig. 4.

The stress distribution in the ground-off NB specimen has been determined by a FE analysis which was performed in ANSYS 12.1/13.0. The quarter-model is shown in Fig. 5a and it includes about 35,000–50,000 elements (hexahedral- and tetrahedron-shaped). In the region, where the crack will be located (position 1′), the mesh is refined. A convergence study with an overall refinement of the mesh (i.e. half element size) showed no significant change of the peak stress. The uncertainties in the determination of the maximum tensile stress in the NB specimens are assumed to be less than 0.1% of its value.

If not specified elsewhere a reference model with the following standard parameters is used for all further investigations: $\lambda = 0.8$, $\omega = 0.15$, $\rho = 0.25$, $\nu = 0.3$, $\alpha = 0.04$, $\beta = 0.05$ and $\gamma = 0.5$, where β is the relative crack size ($\beta = a/R$) and γ represents the crack shape ($\gamma = a/c$). In Fig. 5b the stress field perpendicular

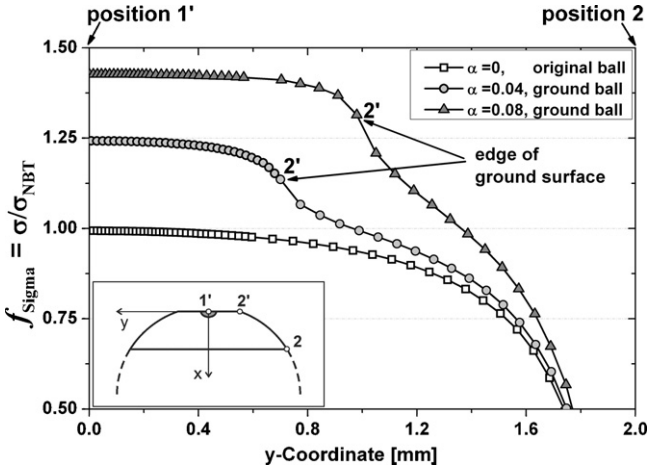

Fig. 6. Stress profile along a path at the surface of the notched ball specimen for the original ball and two different grinding depths α (calculated with FE analysis for the reference model) in relative units. The ratio σ/σ_{NBT} is called f_{Sigma}. The edge of the ground surface for each case is indicated with arrows (position 2′). The maximum stress value in position 1 (position 1′, respectively) increases significantly with α.

to the notch plane (σ_z) at the surface of the reference specimen without crack and after grinding-off a surface layer is illustrated. The stress distribution and its maximum changes due to material removal (compare with Fig. 1).

It is interesting to note, that by modest geometric changes caused by the grinding-off material at the ball apex, the peak stress at the ground surface (position 1′) increases significantly, see Fig. 6. For $\alpha = 0.04$ (the grinding depth is 4% of the ball radius), the peak stress increases almost 25% and for $\alpha = 0.08$ the stress rises strongly again.

In the following, stresses will be described in dimensionless (relative) units, i.e. they will be related to the maximum stress in a perfect NB specimen: $f_{Sigma} = (\sigma/\sigma_{NBT})$. Consider that σ_{NBT} is the first principal stress at position 1, see also Fig. 1. The relative stress at position 1′ depends on the amount of removed material, the Poisson's ratio and the notch geometry.

Apart from the notch length, the notch geometry has a marginal effect on f_{Sigma}, so that the influence of ρ and ω is negligible. The relative stress at position 1′ as a function of α and ν is plotted in Fig. 7. An interpolation function of f_{Sigma} based on 320 calculation points was used for data evaluation.

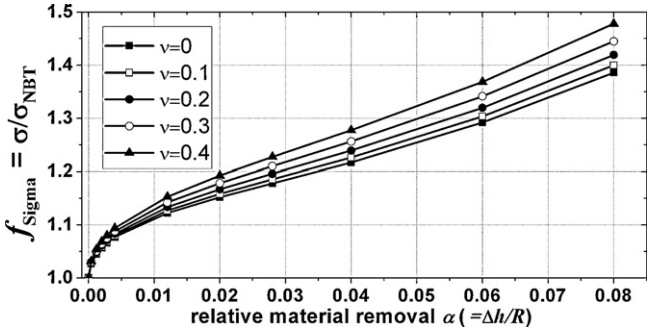

Fig. 7. Relative first principal stress f_{Sigma} at the specimen's surface opposite the notch (position 1′) versus the relative removal α (main influence). Parameter is the Poisson's ratio ν.

Table 1
Overview and considered parameter intervals for the realised parametric FE study.

Dimensionless parameter name	Symbol	Lower limit	Upper limit	Number of design points
Notch length	$\lambda = L_N/D$	0.74	0.82	5
Notch width	$\omega = W_N/D$	0.10	0.15	2
Notch fillet radius	$\rho = R_N/W_N$	0.25	0.40	2
Poisson's ratio	ν	0.15	0.35	5
Grinding depth	$\alpha = \Delta h/R$	0.02	0.05	4
Crack depth	$\beta = a/R$	0.005	0.065	7
Crack aspect ratio	$\gamma = a/c$	0.4	1	7

An interactive applet of the interpolation (regarding λ, ω, ρ, ν and α) can be found in[27] and a fitting function is given in Appendix A. The fitting error is less than 0.25%.

In the experimental practice, to avoid a strong influence of measurement uncertainties, the grinding depth should be deep enough to be outside the parameter range, where the influence of grinding depth in stress is very pronounced. This is the case for $\alpha \geq 0.02$ (see Fig. 7), which used to be the lower limit of our parameter range. Furthermore α should be smaller than 0.05 to ensure an approximate linear course of f_{Sigma} (with respect to the variation of all other notch parameters). Both bounds fit the practical feasibility for commercial bearing ball diameters.

2.4. Numerical determination of the geometric factor Y

In Fig. 8 the stress field (σ_z) at the surface of the reference specimen, including a crack and after grinding-off, is illustrated. For all crack sizes, the amount of the elements along the crack front and their alignment around the crack tip was equal. This was performed with an all hexahedron-meshed cuboid (for mesh details see Fig. 8c).

In every case, the *J*-Integral method, singularity elements along the crack front and a plain strain assumption (effective Young's modulus $E^* = E/(1-\nu^2)$) were deployed for the determination of the stress intensity, more precisely with the formulation $K = \sqrt{E^* \cdot J}$. Correlated to Eq. (2) the geometric factor along the crack front can be expressed with the related *K*, the crack opening stress (σ_z; calculated in the first loading step) at position 1′ and the crack depth *a* (Note: *Y* always refers to the crack depth *a*, see Eq. (2). This means that *a* not the crack width *c* is taken as the typical defect size).

The geometric factor *Y* (see Eq. (2)) was determined in a parameter study (about 20,000 FE runs). The results are used to define two interpolation functions for the geometric factor Y_A and Y_C, respectively. The parameter intervals given in Table 1 for the parametric study have been considered in equidistant steps.

All assumed intervals are realistic in terms of the practical feasibility, if the range of ball diameters is considered to be between 5 and 20 mm. The parameter intervals for the notch geometry are explained in[6] (strength testing). The limits of the Poisson's ratio were chosen concerning typical structural ceramics (silicon carbide: 0.16 and zirconia: 0.34). The limits of the crack geometry parameter, β and γ, are mainly designated through a qualified indentation load (i.e. HK10).

To show the significance of each of the seven varied parameters for the value of the geometric factor *Y*, the trends are shown in Fig. 9. Only one of the seven parameters is varied in each subfigure, for the other six parameters, the values of the reference model were used. The standard crack shape is $\gamma = 0.5$ (ellipse with half axis ratio of 1/2) but for comparison also the curves for a semicircular crack ($\gamma = 1$) are also shown. In subfigure (a) the change of the geometric factor (Y_A and Y_C respectively) with the notch length is illustrated. Y_A decreases much more than Y_C with the notch length, which is reasonable: As a first approximation the ligament is loaded in pure bending. If the ligament *h* gets thinner (i.e. due to a deeper notch) and the crack size is constant the relative stress value at the crack tip at the surface (point C), so Y_C is not influenced. The relative stress value at the deepest point of the crack (point A) decreases for bended specimens, hence, Y_A is affected.

The notch parameters ρ and ω have almost no effect on *Y* (see subfigures (b) and (c)). Plot (d) shows the influence of the Poisson's ratio ν. Y_A and Y_C shift clearly with ν but in the opposite directions.

The tendency of Y_A is decreasing (see plot (e)) for an increasing amount of ground-off material (α).

The relative depth of the crack β has a stronger influence on the geometric factors Y_A and Y_C compared with the relative notch length λ, but both parameters have the same tendencies; see plot (a) and (f). Note that the influence of the analysed parameters on Y_C is weak. Plot (g) shows the course of *Y* in both points with respect to the crack shape (γ). For $\gamma \to 0$, Y_A tends to the analytical value of 1.12 and Y_C tends to become zero. Both facts reflect the analytical solutions for an edge through crack.[28] In summary, the main influences on the geometric factor *Y* are (i) the crack shape (γ) and size (β) and (ii) the ligament geometry (α and λ) with respect to the observed parameter intervals.

An interactive applet for the geometric factors Y_A and Y_C in a NB-specimen can be found in[27] and a fitting function is given in Appendix B. The fits provide an error of less than 1.5%.

Additionally, a semi-analytical approximation for the geometric factor of a semi-elliptical surface crack in the ground NB-specimen based on the Newman–Raju formula is pointed out in Appendix C.

2.5. Data evaluation

Summing it up, the fracture toughness K_C is determined by the stress value in the ground NB-specimen ($\sigma_{NBT} \times f_{Sigma}$) at fracture, the typical crack size *a* and the maximum of the geometric factor *Y* along the crack front, which is influenced by the geometry of the crack and the ligament:

$$K_C = \sigma_{NBT} f_{Sigma} Y_{MAX} \sqrt{a\pi} \quad (3)$$

For data evaluation, the established interpolation functions should always be used to avoid errors due to fitting of the FE results.

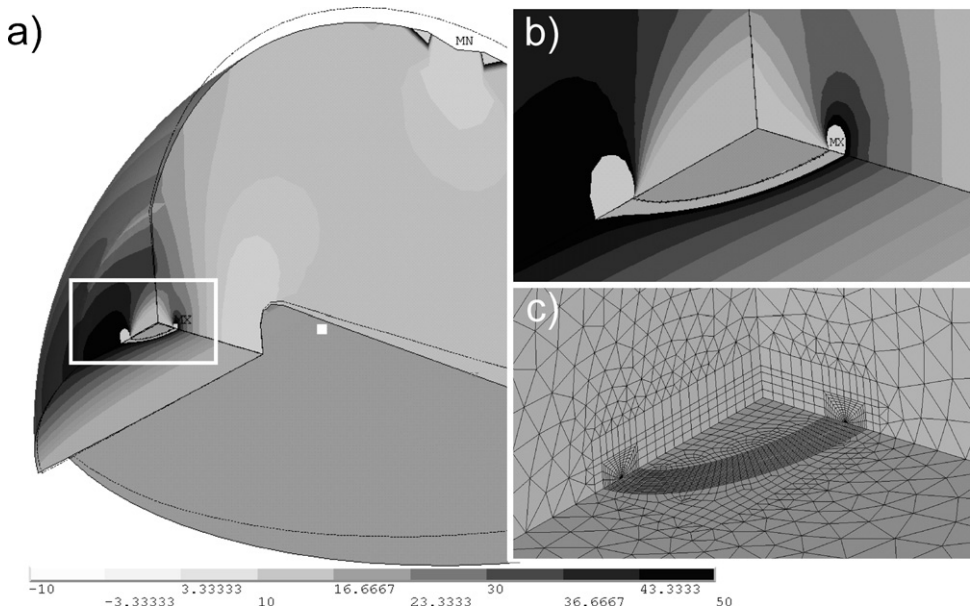

Fig. 8. Stress distribution (σ_z) of a ground-off notched ball specimen with crack: (a) overview and (b) detail of the crack. (c) FE mesh around the crack. For this calculation the reference parameters have been used.

3. Discussion

3.1. The precision of the FE model and the mesh quality

Due to the rising importance of fracture mechanics for proof of safety in structural applications, many different approaches for stress intensity factor (SIF) calculation have been developed. Next to the direct method,[29–32] fitting the stress distribution near the crack tip, three implemented methods are available in the used FE tool ANSYS 13.0 for the linear elastic material behaviour: the "*J*-Integral",[29,33,34] "Virtual Crack Closure Technique" (VCCT)[35–37] and "Crack Opening Displacement" (COD).[29]

To estimate the principle error of these methods the resulting geometric factor Y can be compared to the analytical solution for a fully embedded circular crack in an infinite body ($Y = 2/\pi$). A quarter model of a finite block (full edge length 40 mm × 40 mm × 40 mm) with about 80,000 elements (all hexahedral) and with an embedded crack loaded in Mode I (crack radius $a = 1$ mm) was used. The *J*-Integral method with quarter node collapsed crack tip elements (CTE) provides the best accuracy out of all tested methods (the error is less than 0.01%). This statement can also be found in literature,[29] so this method was chosen for all investigation regarding the NB specimen.

Also a convergence study considering the level of mesh refinement in the NB was carried out for three resulting values: peak stress (position 1′) and the SIF's K_A and K_C. The influences of local mesh refinements of the crack front and the rest of the NB specimen have been observed and compared to the reference model (see Table 1).

There is almost no effect of the crack front mesh refinement on peak stress (first principle stress at position 1′). A global refinement increases the peak stress slightly more (<0.05%).

The influence of mesh refinement on the SIF's is more delicate. The SIF value at the centre of the crack (point A) is not sensitive to crack front refinement. The value at the free surface (point C) is mesh dependent and is continuously decreasing with refinement at the crack front, which is an artifact due to *J*-value determination.[29]

According to this situation the crack front meshing of the reference model seems to be qualified to provide accurate results within an estimated error of 0.5% (note that the principles of stress singularity near the crack tip was always presumed according to Eq. (2), details are discussed below). The mesh refinement apart from the crack front has a negligible effect (∼0.05%) on SIF's.

3.2. Influence of the Poisson's ratio ν on the geometric factor

The dependence of the geometric factors Y on the Poisson's ratio ν for small ($\beta = 0.005$) and large ($\beta = 0.05$) cracks respectively (as determined in our FE analysis) is shown in Fig. 10. Also shown are the solution of Newman and Raju which is only carried out for $\nu \sim 0.3$. But for a precise determination of the geometric factor, the influence of the Poisson's ratio has also to be considered. (Note: own FE analysis of a rectangular beam under tension with a semi-elliptical surface crack showed that the variation of ν indicates the same tendencies as plotted in Fig. 10 for the NB-specimen.)

3.3. Deviations of the crack shape from the semi-elliptical shape

In our calculations (and also in the calculations of Newman and Raju) it is assumed that the crack is "perfectly"

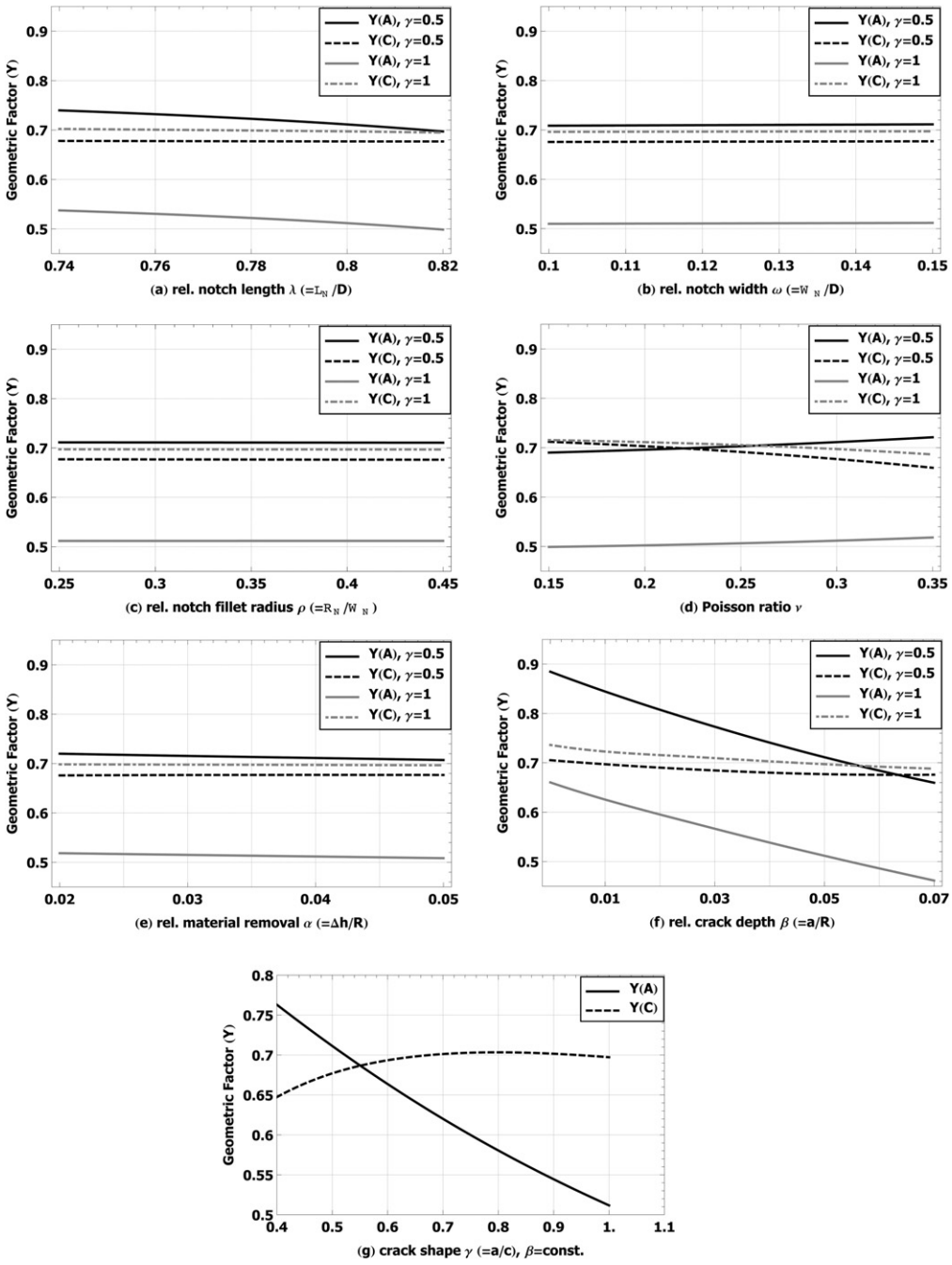

Fig. 9. Parametric study of the influence of model parameters on the geometric factor Y (in each case for point A and point C) in the dimensionless reference model. (a–c) Variation of the notch geometry (λ, ω, and ρ), (d) variation of the Poisson's ratio ν, (e) variation of the removed material α and (f–g) variation of the crack geometry β and γ.

semi-elliptically shaped. This assumption is also made in the standards for SCF toughness measurements. In reality, this is normally not the case. Even if the initial Knoop crack was perfectly semi-elliptical, grinding the surface layer of the crack will leave another contour. This case has been studied in,[28] where – for worst case assumption – the differences in the geometric factors are less than: ±4% in point A and less than ±2% in point C for cracks having the same aspect ratio a/c.

3.4. Stress singularity at the free surface

The maximum of the Y-values along the crack front is always located either at point A or at point C (see Fig. 3) and never between them,[22,23,25] so just those two distinguished points have to be observed.

Generally at the free surface (at point C) the stress singularity is not proportional to $r^{-1/2}$ (with r as the distance from the crack tip) according to Fett,[38] Hutar[30,32] and de Matos.[39]

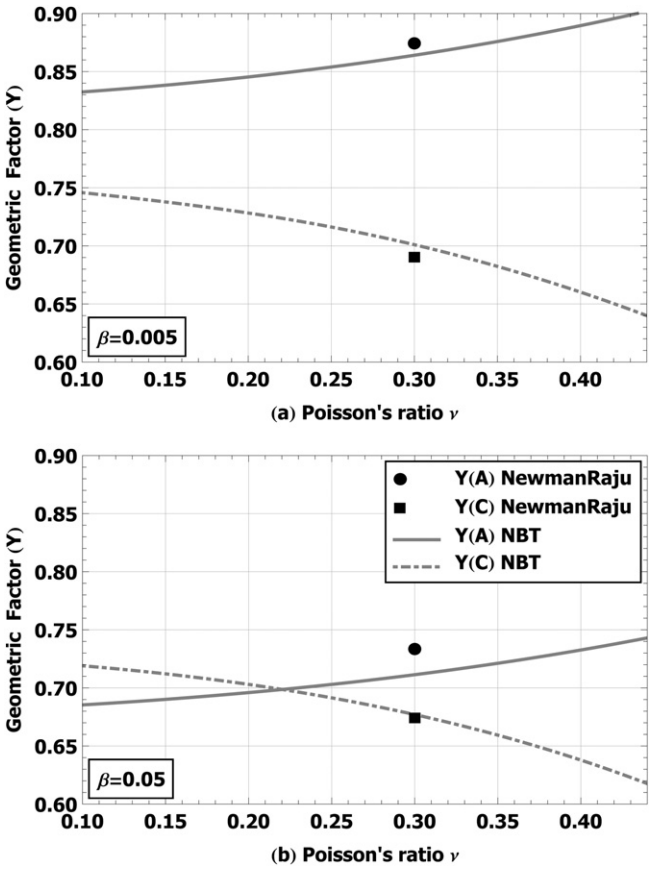

Fig. 10. Comparison of the *Y*-solutions of the own FE analysis (NBT) and the Newman–Raju formula plotted versus the Poisson's ratio ν for (a) small cracks ($\alpha = 0.5\%$) and (b) big cracks ($\alpha = 5\%$).

More precisely, the *K*-concept is therefore not valid at point C and it can only be used as an approximate approach. This effect is pronounced, if the crack intersects the surface perpendicular ($\phi \approx 90^\circ$) and the Poisson's ratio is unequal to zero (the Poisson's ratio also influences the thickness of this boundary layer).

Therefore the ASTM standard for the SCF-method[16] instructs to use flat crack shapes with $Y_A > Y_C$, i.e. the maximum of *Y* should be positioned at point A. In practice, the easiest way to realise this is to increase the grinding depth Δh. This has several useful effects: the intersection angle ϕ gets smaller and the crack shape becomes flatter. The condition $Y_A > Y_C$ is fulfilled for flat crack shapes (the limit is at $\gamma = 0.6 \div 0.8$, which depends on the crack size β).

On the other hand the ISO-standard for the SCF-method[17] determines that the greater one out of both *Y*-value should be used for fracture toughness calculation. For this, two conditions have to be considered: (1) the crack has to be nearly semi-elliptical and (2) the datum has to be rejected, if $Y_A < Y_C$ and the fracture could be caused by preparation damage or corner pop-ins at the surface-point C.

4. Concluding remarks

The standardized SCF-method for fracture toughness measurements on ceramics is modified and applied to a new specimen type, the notched ball. Compared to the NBT strength testing procedure, a modification of the geometry of the notched ball is necessary. Grinding-off the plastic zone produced by the Knoop indentation changes the peak stress at the ball apex. A dimensionless stress correction factor was evaluated by numerical analysis.

The geometry factor *Y* was calculated for a wide range of notch and crack geometries by FEA. These results are compared with the Newman–Raju formula (generalized solution used in the standard SCF-method). An interpolation function of the new results takes the Poisson's ratio into account, which is necessary for the characterisation of other structural ceramics.

If the crack aspect ratio is $a/c < 0.6$, the notched ball specimen also favours crack instability at the deepest point (point A), which is a well defined situation in fracture mechanics, therefore flat surface cracks should be aimed. With typical indentation crack sizes (that can be achieved for advanced ceramics) the new method may be applied to balls with diameters between 2 mm and 20 mm.

In the second part of the paper, which will be published soon, the experimental procedure of the new fracture toughness test are described in detail, measurement uncertainties are discussed and experimental results on silicon nitride balls are presented. The results fit well to measurement results determined using other standard testing procedures on bending test specimens.

Acknowledgements

Financial support by the Austrian Federal Government (in particular from the Bundesministerium für Verkehr, Innovation und Technologie and the Bundesministerium für Wirtschaft, Familie und Jugend) and the Styrian Provincial Government, represented by Österreichische Forschungsförderungsgesellschaft mbH and by Steirische Wirtschaftsförderungsgesellschaft mbH, within the research activities of the K2 Competence Centre on "Integrated Research in Materials, Processing and Product Engineering", operated by the Materials Center Leoben Forschung GmbH in the framework of the Austrian COMET Competence Centre Programme, is gratefully acknowledged.

Appendix A. Fit function for the maximum tensile stress in the NB specimen (at position 1′) after material removal (an interactive applet with the original interpolation can be found in [27])

The results of the FEM-calculations were fitted to a polynomial. It is intended to keep the fit function simple and that the deviation of the fit function from the FE results should be less than 1%. The stress is given in relative units (normalised with the maximum tensile stress in a NB specimen without surface material removal). The relative stress significantly depends on the relative amount of material removed ($\alpha = \Delta h/R$), the relative notch length ($\lambda = 1 - h/(2R)$) and on the Poisson's ratio (ν). *R* is

Table A1
Coefficients for the fitting function for the stress factor (see Eq. (A.1)).

Indices	Fit coefficients (with $z_0 = 1.07844$)			
	a	b	c	d
10	−0.591634	2.37305	2.8519	2.74222
11	2.6177	4.54232	2.65985	1.65029
12	−2.06407	−19.5959	−3.41503	4.938
20	−1.39017	3.50268	−8.0687	9.59176
21	4.62443	6.77471	−9.46501	6.54502
22	−3.41374	−44.9503	11.1753	24.7514
30	3.08148	8.73812	20.9244	10.3407
31	−7.41486	17.1121	23.2816	3.63325
32	4.803	−164.037	−24.6965	18.151

the radius of the ball. The influences of the relative notch width and of the relative notch fillet radius are weak.

The general fit function for f_{Sigma} is given in Eq. (A.1) and the needed coefficients in Table A1. The fitting error is less than 0.25%.

$$\begin{aligned} f_{\text{Sigma}}(\lambda, \omega, \rho, \nu, \alpha) &= z_0 + \alpha(a_{10} + a_{11}\lambda + a_{12}\lambda^2) \\ &\times (b_{10} + b_{11}\omega + b_{12}\omega^2)(c_{10} + c_{11}\rho + c_{12}\rho^2) \\ &\times (d_{10} + d_{11}\nu + d_{12}\nu^2) + \alpha^2(a_{20} + a_{21}\lambda + a_{22}\lambda^2) \\ &\times (b_{20} + b_{21}\omega + b_{22}\omega^2)(c_{20} + c_{21}\rho + c_{22}\rho^2) \\ &\times (d_{20} + d_{21}\nu + d_{22}\nu^2) + \alpha^3(a_{30} + a_{31}\lambda + a_{32}\lambda^2) \\ &\times (b_{30} + b_{31}\omega + b_{30}\omega^2)(c_{30} + c_{31}\rho + c_{32}\rho^2) \\ &\times (d_{30} + d_{31}\nu + d_{32}\nu^2) \end{aligned} \tag{A.1}$$

Appendix B. Fit function of the geometric factor Y in the ground NB-specimen (an interactive applet with the original interpolation can be found in [27])

The numerical values of the geometric factor Y_A and Y_C can be fitted in terms of the parameters λ, ν, α, β and γ. The influence of the notch parameters ω and ρ is negligible (consider Fig. 9); the reference values were used. The general fitting function – for Y_A and Y_C – is shown in Eq. (B.1). The needed coefficients are given in Table B1 The fitting error is less than 1.5% in point C and less than 1% in point A.

$$\begin{aligned} &Y(\lambda, \omega = 0.12, \rho = 0.25, \nu, \alpha, \beta, \gamma) \\ &= z0 + \gamma^{0.2}(a_{10} + a_{11}\lambda + a_{12}\lambda^2)(b_{10} + b_{11}\nu + b_{12}\nu^2) \\ &\quad \times (c_{10} + c_{11}\beta + c_{12}\beta^2)(d_{10} + d_{11}\alpha + d_{12}\alpha^2) \\ &\quad + \gamma(a_{20} + a_{21}\lambda + a_{22}\lambda^2)(b_{20} + b_{21}\nu + b_{22}\nu^2) \\ &\quad \times (c_{20} + c_{21}\beta + c_{22}\beta^2)(d_{20} + d_{21}\alpha + d_{22}\alpha^2) \\ &\quad + \gamma^2(a_{30} + a_{31}\lambda + a_{32}\lambda^2)(b_{30} + b_{31}\nu + b_{32}\nu^2) \\ &\quad \times (c_{30} + c_{31}\beta + c_{32}\beta^2)(d_{30} + d_{31}\alpha + d_{32}\alpha^2) \end{aligned} \tag{B.1}$$

Appendix C. A semi-analytical approximation for the geometric factor of a semi-elliptical surface crack in the ground NB-specimen

More than 30 years ago Newman and Raju have derived an approximation for the geometric factor of a semi-elliptical surface crack in a bended rectangular bar. This solution is used for data evaluation in the standard SCF-method. The geometric factor of a semi-elliptical surface crack in the NB specimen having a ground surface can also be found – in a semi-analytical approximation – using the Newman and Raju solution. In the ligament of the ground NB specimen the course of the first principal stress – perpendicular to the surface – is almost linear decreasing (see Fig. C1). In other words the stress field is very similar to that of a bended rectangular bar. Therefore it is possible to define a bending bar, which has the same slope of the stress field as the ground NB specimen. The thickness of the bar is h_{eq} and, for simplicity, the half width b is defined to be $b = h_{\text{eq}}$ (see Fig. C1).

The equivalent beam thickness h_{eq} depends on the ligament geometry (mainly on α and λ) and the crack depth a. The stress distribution is nearly linear in the relevant region, i.e. over typical ranges of the crack depth a (for $0 \le a \le 0.25h'$).

A fitting function of the equivalent thickness h_{eq} – based at our FE results – is given in Eq. (C.1)–(C.3).

The relations have been derived by computing the stresses in the ligament of the actual (ground) notched ball specimen in

Table B1
Coefficients for the fitting function for the geometric factor (see Eq. (B.1)).

Indices	Point A (with $z_0 = 1.259$)				Point C (with $z_0 = -1.46387$)			
	a	b	c	d	a	b	c	d
10	−1.16634	0.84972	0.482606	1.23491	1.30137	1.3381	0.785785	2.27784
11	0.0191434	1.97075	28.3316	−3.02365	−0.0735881	0.315134	−0.0836458	−0.0569606
12	0.208143	−7.32415	−113.135	2.21254	−0.364722	−3.18661	1.64754	0.0292848
20	0.128234	1.33431	1.77848	1.18249	0.632871	0.983236	−0.247442	5.72478
21	−0.0209168	−1.41052	−11.5363	−10.7237	−0.259051	1.25891	−0.511638	2.34767
22	−0.153399	8.01953	64.7578	7.67749	−0.161234	−12.3825	1.13783	−1.71875
30	0.355241	3.16874	−1.3068	0.0796565	3.05859	−0.0162337	−1.20701	−1.53108
31	−0.217446	−2.99067	5.18989	−0.66641	−3.10434	−0.0538943	−14.9341	11.5755
32	−0.94953	17.7899	−29.3815	0.454138	2.0719	0.577001	84.2279	−8.59851

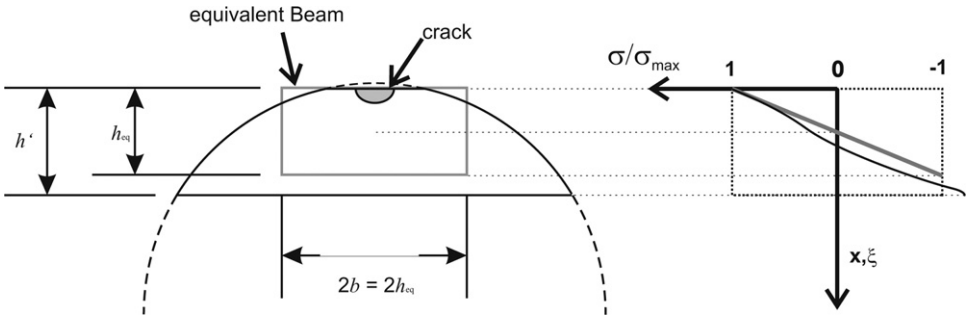

Fig. C1. The stress field in a bended beam of thickness h_{eq} and of width $2h_{eq}$ is almost equal to that of the stress field in a ground NB specimen (at least at the surface, where high stresses occur).

crack depth direction x(or $\xi = x/h'$) for several ball-notch configurations. For further information see.[18,40]

$$h_{eq} = f_h h' \tag{C.1}$$

with

$$f_h = \frac{-2a/h'}{\sigma_{z,Lig}(\xi = a/h') - 1} \tag{C.2}$$

and

$$\sigma_{z,Lig} = 1 + (m_0\lambda + m_1\lambda^2)n_0\xi + (m_2\lambda + m_3\lambda^2)n_1\xi^2 \tag{C.3a}$$

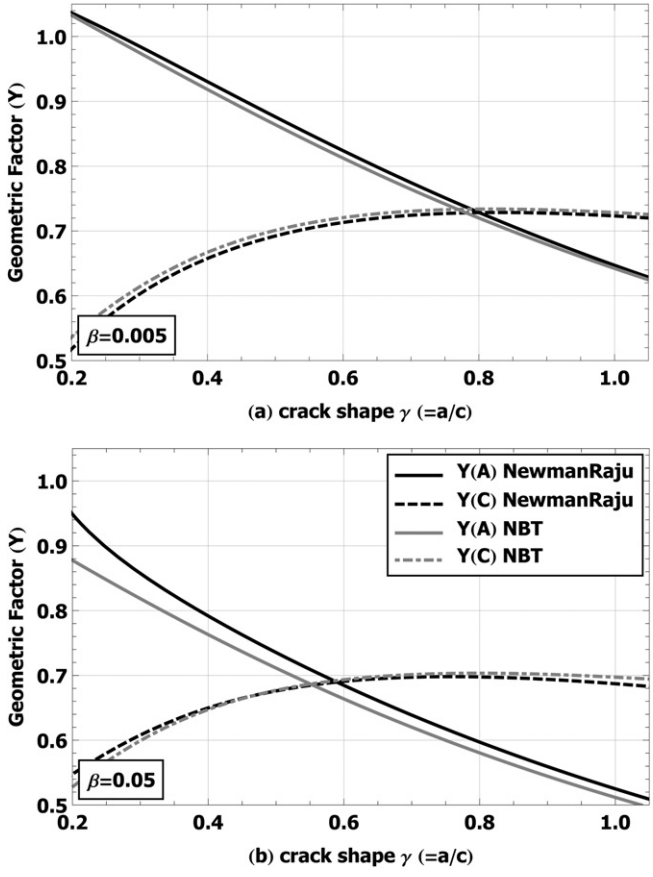

Fig. C2. Comparison of the geometric factors determined by FE-calculations and by a semi analytical approach based on the Newman–Raju formula, plotted are values of the factor versus the crack shape γ for (a) small cracks ($\beta = 0\,5\%$) and (b) big cracks ($\beta = 5\%$).

with

$$m_0 = -2.54721 \quad m_1 = 2.17406 \quad m_2 = 5.63419 \quad m_3 = -6.07159$$
$$n_0 = 3.93603 \quad n_1 = 3.00221 \tag{C.3b}$$

Due to the modification discussed above and the approximations of the Newman and Raju, the determination of the geometric factor of a semi-elliptical crack in a ground NB specimen has an unknown uncertainty. Newman and Raju claim that their fitting function provided has a maximum error of ±5% according to their FE results.[25] In addition, they specified their FE accuracy with ±3% compared to the analytical solution in terms of a completely embedded circular crack.[24,26] All their calculations have been made for a Poisson's ratio of $\nu = 0.3$. A direct comparison of the Newman and Raju formula and with own FE analysis for a semi-elliptical surface crack in a rectangular beam under pure tension showed an error of less than ±3% for $\nu = 0.3$.

For the NB model, a comparison of the Y-courses of our (very accurate) NBT-FE analysis with the approximations based on the Newman and Raju formula is shown in Fig. C2 (Note: all of our FEM values outside of $0.4 \leq \gamma \leq 1$ are extrapolated). For relative small crack sizes ($\beta = 0.005$, see Fig. C2a) both solutions agree surprisingly well; the maximum deviation is less than ±1.2%. For bigger cracks ($\beta = 0.05$, see Fig. C2b) the maximum error for Y_A rises up to 2.9%, but for Y_C the difference between both solutions is still less than 1% for all analysed crack sizes. Generally, the agreement of the FE-results with the approximations based on the Newman and Raju formula and their tendencies is good but the agreement decreases with bigger relative crack sizes.

In general the semi-analytical calculations of Newman and Raju give the same trend with the crack shape as our FE calculations but they are only valid for $\nu = 0.3$. Our FE-solution can be used in the range of Poisson's ratio of interest (see Table 1).

References

1. Köttritsch H. *Science report: development centre steyr*. Steyr: SKF Österreich AG; 2007.
2. Wang L, Snidle RW, Gu L. Rolling contact silicon nitride bearing technology: a review of recent research. *Wear* 2000;**246**:159–73.
3. Supancic P, Danzer R, Harrer W, Wang Z, Witschnig S, Schöppl O. Strength tests on silicon nitride balls. *Key Engineering Materials* 2009;**409**:193–200.
4. Supancic P, Danzer R, Wang Z, Witschnig S, Schöppl O. The Notched Ball Test – a new strength test for ceramic spheres. In: *9th international*

symposium on ceramic materials and components for energy and environmental applications. Shanghai: The American Ceramic Society; 2009. p. 67–75.
5. Supancic P, Danzer R, Witschnig S, Polaczek E. The strength of ceramic balls – the Notched Ball Test. In: *18th European conference on fracture*. 2010.
6. Supancic P, Danzer R, Witschnig S, Polaczek E, Morrell R. A new test to determine the tensile strength of brittle balls – the Notched Ball Test. *Journal of the European Ceramic Society* 2009;**29**:2447–59.
7. Wereszczak AA, Kirkland TP, Jadaan OM. Strength measurement of ceramic spheres using a diametrally compressed "C-Sphere" specimen. *Journal of the American Ceramic Society* 2007;**90**:1843–9.
8. ASTM 2094-08. *Standard specification for silicon nitride bearing Balls*. American Society for Testing and Materials; 2008.
9. Lube T. Indentation crack profiles in silicon nitride. *Journal of the European Ceramic Society* 2001;**21**:211–8.
10. Miyazaki H, Hyuga H, Yishizawa Y-I, Hirao K, Ohji T. Relationship between fracture toughness determined by surface crack in flexure and fracture resistance measured by indentation fracture for silicon nitride ceramics with various microstructures. *Ceramics International* 2009;**35**:493–501.
11. Niihara K, Morena R, Hasselman DPH. Further reply to "comments on elastic/plastic indentation damage in ceramics: the median/radial crack system". *Journal of the American Ceramic Society* 1982;**65**:C-116.
12. Anstis GR, Chantikul P, Lawn BR, Marshall DB. A critical evaluation of indentation techniques for measuring fracture toughness. I. Direct crack measurements. *Journal of the American Ceramic Society* 1981;**64**:533–8.
13. CEN EN 14425-5. *Fine ceramics (advanced ceramics, advanced technical ceramics) – determination of fracture toughness of monolithic ceramics at room temperature by the single-edge vee-notched beam (SEVNB) method*; 2005.
14. Damani R, Gstrein R, Danzer R. Critical notch root radius in SENB-S fracture toughness testing. *Journal of the European Ceramic Society* 1996;**16**:695–702.
15. Damani R, Schuster C, Danzer R. Polished notch modification of SENB-S fracture toughness testing. *Journal of the European Ceramic Society* 1997;**17**:1685–9.
16. ASTM C 1421-01b. *Standard test methods for determination of fracture toughness of advanced ceramics at ambient temperature*. American Society for Testing and Materials; 2001.
17. ISO 18756. *Fine ceramics (advanced ceramics, advanced technical ceramics) – determination of fracture toughness of monolithic ceramics at room temperature by the Surface Crack in Flexure (SCF) method*; 2003.
18. Witschnig S. *Zähigkeitsmessung an keramischen Kugeln. Institut für Struktur- und Funktionskeramik*. Diploma Thesis. Leoben: Montanuniversitaet Leoben; 2010.
19. Munz D, Fett T. *Ceramics – mechanical properties, failure behaviour, materials selection*. Berlin: Springer; 2001.
20. Lawn BR. *Fracture of brittle solids*. second ed. Cambridge: Cambridge University Press; 1993.
21. Murakami Y. *Stress intensity factors handbook*. Oxford: Pergamon Press; 1987–2001.
22. Quinn GD, Gettings RJ, Kübler J. Fracture toughness by the surface crack in flexure (SCF) method: results of the VAMAS round robin. *Ceramic Engineering and Science Proceedings* 1994;**15**:846–55.
23. Quinn GD, Kübler J, Gettings RJ. Fracture toughness of advanced ceramics by the surface crack in flexure (SCF) method: a VAMAS round robin. VAMAS Report No. 17. Report 1994.
24. Newman JC, Raju IS. Analysis of surface cracks in finite plates under tension or bending loads NASA. Report TP-1578; 1979.
25. Newman JC, Raju IS. An empirical stress-intensity factor equation for the surface crack. *Engineering Fracture Mechanics* 1981;**15**:185–92.
26. Raju IS, Newman JC. Improved stress-intensity factors for semi-elliptical surface cracks in finite-thickness plates NASA. Report TM-X-72825; 1977.
27. http://www.isfk.at.
28. Fett T, Munz D. *Stress intensity factors and weight functions*. Southampton UK and Boston USA: Computational Mechanics Publications; 1997.
29. Anderson TL. *Fracture mechanics – fundamentals and applications*. Boca Raton, FL: CRC Press; 2005.
30. Hutar P, Náhlík L, Knésl Z. Quantification of the influence of vertex singularities on fatigue crack behavior. *Computational Materials Science* 2009;**45**:653–7.
31. Hutar P, Náhlík L, Knésl Z. The effect of a free surface on fatigue crack behaviour. *International Journal of Fatigue* 2010;**32**:1265–9.
32. Hutar P, Sevcík M, Náhlík L, Zouhar M, Seitl S, Knésl Z, et al. Fracture mechanics of the three-dimensional crack front: vertex singularity versus out of plain constraint descriptions. *Procedia Engineering* 2010;**2**:2095–102.
33. Banks-Sills L. Application of the finite element method to linear elastic fracture mechanics. *Applied Mechanics Reviews* 1991;**44**:447–61.
34. Courtin S, Gardin C, Bézine G, Ben Hadj Hamouda H. Advantages of the J-integral approach for calculating stress intensity factors when using the commercial finite element software ABAQUS. *Engineering Fracture Mechanics* 2005;**72**:2174–85.
35. Krueger R. Virtual crack closure technique: history, approach, and applications. *Applied Mechanics Reviews* 2004;**57**:109–43.
36. Leski A. Implementation of the virtual crack closure technique in engineering FE calculations. *Finite Elements in Analysis and Design* 2007;**43**:261–8.
37. Okada H, Kawai H, Araki K. A virtual crack closure-integral method (VCCM) to compute the energy release rates and stress intensity factors based on quadratic tetrahedral finite elements. *Engineering Fracture Mechanics* 2008;**75**:4466–85.
38. Fett T. *Stress intensity factors – T-stresses – weight functions. Supplement volume (IKM 55)*. Karlsruhe: KIT Scientific Publishing; 2009.
39. de Matos PFP, Nowell D. The influence of the Poisson's ratio and corner point singularities in three-dimensional plasticity-induced fatigue crack closure: a numerical study. *International Journal of Fatigue* 2008;**30**:1930–43.
40. Lube T, Witschnig S, Supancic P. Fracture toughness of ceramic balls. In: *18th European conference on fracture*. 2010.